Bioprinting 31 (2023) e00269

Contents lists available at ScienceDirect

Bioprinting

journal homepage: www.sciencedirect.com/journal/bioprinting

Versatile and non-cytotoxic GelMA-xanthan gum biomaterial ink for extrusion-based 3D bioprinting

Filippo Iervolino [a,1], Beatrice Belgio [b,1], Aurora Bonessa [a], Federica Potere [b], Raffaella Suriano [a,*], Federica Boschetti [b], Sara Mantero [b], Marinella Levi [a]

[a] +LAB, Department of Chemistry, Materials and Chemical Engineering "Giulio Natta", Politecnico di Milano, Milano, Italy
[b] LaBS, Department of Chemistry, Materials and Chemical Engineering "Giulio Natta", Politecnico di Milano, Milano, Italy

ARTICLE INFO

Keywords:
Direct ink writing
Rheological properties
Printability
Cytotoxicity
GelMA
Xanthan gum

ABSTRACT

Extrusion-based 3D bioprinting allows the 3D printing of bioinks, composed of cells and biomaterials, to mimic the complex 3D hierarchical structure of native tissues. Successful 3D bioprinting requires bioinks with specific properties, such as biocompatibility, printability, and biodegradability according to the desired application. In the present work, we aimed at developing a new versatile blend of gelatin methacryloyl-xanthan gum (GelMA-XG) suitable for extrusion-based 3D bioprinting with a straightforward process. To this end, we first optimized the process of gelatin methacryloyl (GelMA) synthesis by investigating the impact of different buffer solutions on the degree of functionalization, swelling degree, and degradation rate. The addition of xanthan gum (XG) enabled further tuning of biodegradability and an improvement of GelMA printability. Specifically, an optimal concentration of XG was found through rheological characterization and printability tests. The optimized blend showed enhanced printability and improved shape fidelity as well as its degradation products turned out to be non-cytotoxic, thus laying the foundation for cell-based applications. In conclusion, our newly developed biomaterial ink is a promising candidate for extrusion-based 3D bioprinting.

1. Introduction

3D cell cultures based on the fabrication of *in vivo*-like microenvironment able to accurately mimic the native extracellular matrix (ECM) have demonstrated various advantages over 2D cell culture in the last two decades [1]. The introduction of extrusion-based 3D bioprinting has revolutionized the assembly process of 3D cell cultures thanks to the possibility of printing bioinks made of cells and biomaterials with a precise pattern [2]. This allows the creation of complex biological functional architectures with precise control over the position of cells and biomaterials [3–5]. The choice of bioinks to be printed is crucial, as the final chemical, structural, and mechanical properties of the construct depend on the selected bioink [6–8]. Besides the various requirements needed for every scaffold (e.g., biocompatibility, bioactivity, biodegradation, and adequate mechanical and structural properties), bioinks should also exhibit a suitable rheological behavior to be successfully extruded and printed while retaining the structure imparted by the printing process.

Several naturally derived materials, such as gelatin and sodium alginate, have been extensively employed for the development of 3D printed scaffolds [9]. Among these materials, gelatin has been commonly selected due to the presence of the three-amino acid sequence Arginine–Glycine–Aspartate (RGD), which promotes cell attachment and adhesion [10]. The gelation of gelatin in an aqueous solution can be obtained below the helix-to-coil transition temperature, at which the formation of a 3D network due to the rearrangement of random coils into triple helices occurs [11]. At physiological temperatures, however, gelatin is characterized by poor stability. Therefore, to achieve greater gel stability and enhance printability, gelatin has been often functionalized with methacrylamide side groups through the reaction of methacrylic anhydride with amine groups. This reaction allows the initiation of a radically covalent crosslinking between the polypeptide chains of gelatin resulting in the creation of gelatin-methacryloyl (GelMA), which can be photo-crosslinked to obtain a stable structure at physiological temperature. Moreover, GelMA showed superior printability properties

* Corresponding author.
E-mail addresses: filippo.iervolino@polimi.it (F. Iervolino), beatrice.belgio@polimi.it (B. Belgio), aurorabonessa@icloud.com (A. Bonessa), federica.potere@polimi.it (F. Potere), raffaella.suriano@polimi.it (R. Suriano), federica.boschetti@polimi.it (F. Boschetti), sara.mantero@polimi.it (S. Mantero), marinella.levi@polimi.it (M. Levi).
[1] contributed equally to the work.

https://doi.org/10.1016/j.bprint.2023.e00269
Received 28 October 2022; Received in revised form 1 March 2023; Accepted 17 March 2023
Available online 20 March 2023

when compared to gelatin and other bioinks [12]. In addition, the crosslinking process enables to tune rheological and mechanical properties of GelMA hydrogels by varying the polymer and initiator concentration, the degree of functionalization, and UV polymerization conditions [13] to better replicate the native properties of the tissue [14]. For all these reasons, GelMA has been used for many applications [15] including cellular encapsulation for bioprinting [16]. However, pure GelMA showed a narrow printability window depending on specific printing parameters, such as temperature. Li et al. showed that GelMA hydrogels (5% w/v concentration in PBS) printed at 29 °C provided a good accuracy as desired in the multichannel structures for nerve guidance conduits, keeping fixed the other printing parameters such as the UV light exposure time [17]. Whereas, at different temperatures, i.e., 24 °C and 45 °C, the same channels did not show the same shape fidelity as at 29 °C. The role of the extruding temperature in the nozzle from 10 °C to room temperature and of GelMA hydrogel concentrations from 5 to 15% w/v was also evaluated by Janmanleki and coworkers, maintaining other printing parameters constant [18]. In their work, GelMA with a concentration of 10% w/v extruded at 15 °C was found to be the hydrogel with the optimal response in terms of printable filament shape and uniformity, even though the biodegradability and the cell biocompatibility were reduced when compared to the 10% w/v hydrogel extruded at room temperature. Hence, nowadays fabricating 3D printed GelMA structures able to be printable at room temperature and, once printed, maintaining shape retention, proper biodegradability, and cell biocompatibility is still particularly challenging. For this reason, various strategies were explored to improve printability such as the 3D printing of GelMA on a cooled platform to increase the shape fidelity and the resolution of the printed constructs [19]. Among these, the combination of GelMA with other polymers seems to be a viable approach to address printability issues, thus improving material extrudability and high shape fidelity of the printed construct [20]. For instance, a biomaterial ink composed of carboxymethylcellulose sodium, xanthan gum (XG), and GelMA demonstrated excellent shape fidelity preventing filament collapse [21]. Similarly, Garcia-Cruz et al. proposed that XG could be methacrylated and combined with GelMA to obtain a stable bioink with enhanced printability properties [22].

In the present study, we aimed at developing a functional innovative biomaterial ink composed of a GelMA-XG blend for extrusion-based 3D bioprinting with an easy procedure. The newly developed ink was required to have a tunable biodegradability to ensure its versatility, thus allowing its use for various bioprinting applications, such as active drug delivery or tissue engineering. To this end, GelMA was synthesized using two different buffer solutions to obtain two different degrees of GelMA methacrylation and swelling ratio and degradation rate were investigated. In addition, a suitable ink blend that led to enhanced printability and cell viability was identified through rheological characterization, printing tests, and in vitro indirect cytotoxicity assay.

2. Materials and methods

2.1. Materials

Gelatin (from porcine skin, gel strength ~175 g Bloom, type A), methacrylic anhydride (MA), 2-hydroxy-4′-(2-hydroxyethoxy)-2-methylpropiophenone (Irgacure 2959), xanthan gum (XG), phosphate-buffered saline tablets (PBS) and carbonate-bicarbonate buffer capsule (CB) were purchased from Sigma Aldrich and used as received. High glucose Dulbecco's Modified Eagle's Medium (DMEM) and penicillin/streptomycin antibiotics were obtained from Gibco™ (Thermo Fisher Scientific), whereas L929 cells, a murine fibroblast cell line, (Catalog No. CCL-1™) and fetal bovine serum were acquired from American Type Culture Collection. Finally, alamarBlue Assay for Cell Viability was purchased from Invitrogen™ (Thermo Fisher Scientific).

2.2. GelMA synthesis mechanism

GelMA was synthesized in PBS (GelMA_PBS) and CB (GelMA_CB) buffer solutions according to the previously reported method (Fig. 1) [15, 23]. Briefly, 5 g of gelatin type A was dissolved in 50 mL of either PBS 1X (pH = 7.4) or 0.1 M CB solution (pH = 9) at 50 °C for 1.5 h for total solubilization. Next, 0.5 mL of methacrylic anhydride (MA) was added to the gelatin solution. The reaction was carried on for 3 h under vigorous magnetic stirring. For PBS buffer, a quenching was performed to stop the reaction adding 200 ml of PBS to the solution. When using CB buffer solution, the reaction was stopped by adjusting the pH to 7.4 adding 6 M hydrochloric acid. Then, the solution was dialyzed for 3 days, and the dialysis water was changed once a day. Finally, a freeze-drying process was performed at 0.3 bar for 72 h and the material was stored at 4 °C.

2.3. Nuclear magnetic resonance

The proton nuclear magnetic resonance (^{1}H NMR) spectrometry was used to determine GelMA_PBS and GelMA_CB degree of functionalization (DOF), also known as methacrylation degree. To perform the analyses, 10 mg of the synthesized GelMA was dissolved in 0.75 mL of deuterium oxide (D_2O) containing 0.75 wt% of trimethylsilyl propanoic acid (TMSP). The spectra were registered on a Bruker spectrometer AMX 400 MHz (Bruker BioSpin, Rheinstetten, Germany). Two methods were used for deriving the final DOF. The first method implied the use of TMSP as an internal standard (0 ppm), while the second method used the lysine signals (7.0–7.5 ppm) as an internal reference to normalize the amine signals (2.9 ppm) of methacrylated lysine. The DOF was calculated using Equations (1) and (2).

$$Degree\ of\ functionalization\ (DOF_{TMSP}) = \frac{\int methacryl}{\int TMSP} \bullet \frac{9H}{1H} \bullet \frac{n\ TMSP\ [mmol]}{m\ GelMA\ [g]} \tag{1}$$

$$Degree\ of\ functionalization\ \left(DOF_{lys}\right) = 1 - \frac{integration\ of\ lysine\ signal\ from\ GelMA}{integration\ of\ lysine\ signal\ from\ Gelatin} \tag{2}$$

DOF_{TMSP} was calculated with the double bond protons of the methacryl groups, located at 6.5−5.0 ppm and nominally integrated for two protons, and normalized on the TMSP integral, located at 0 ppm, and integrated for nine protons [24]. For the methacrylate amount, the integral of the signal with the highest chemical shift, located at 6.3−5.9 ppm was called $\int$ methacryl and it was integrated for one proton [15]. For the total amount of methacryl groups (methacrylate and methacrylamide), the integral of the signal with a chemical shift of 5.9−5.5 ppm was added to $\int$ methacryl [24]. It is caused by an overlay of signals belonging to one proton of the methacrylate and one proton of the methacrylamide groups and is therefore nominally integrating for one proton as well [24].

DOF_{lys} was calculated on ^{1}H NMR spectra normalized to the lysine integral, located at 7.5−6.9 ppm and integrated for five protons. The lysine methylene signals of nonmodified gelatin and gelatin derivatives, located at 2.95−2.8 ppm were integrated and compared as reported in equation (2) [24].

2.4. TNBS assay

The Habeeb method with trinitrobenzene sulfonate (TNBS) was used as an additional method to evaluate functionalization degree. Briefly, gelatin, GelMA_PBS, and GelMA_CB were dissolved in 0.1 M CB reaction buffer with 5 mg/ml and 10 mg/ml concentration for the gelatin and the modified gelatin, respectively. TNBS 5% w/v in methanol was diluted in a 0.1 M CB reaction buffer to reach a concentration of 0.01% w/v. Then 0.5 ml of the TNBS solution was added to the pure gelatin and modified gelatin samples. Therefore, to let the TNBS react with the non-modified lysine groups in each sample, they incubated for 2 h at 37 °C in the dark

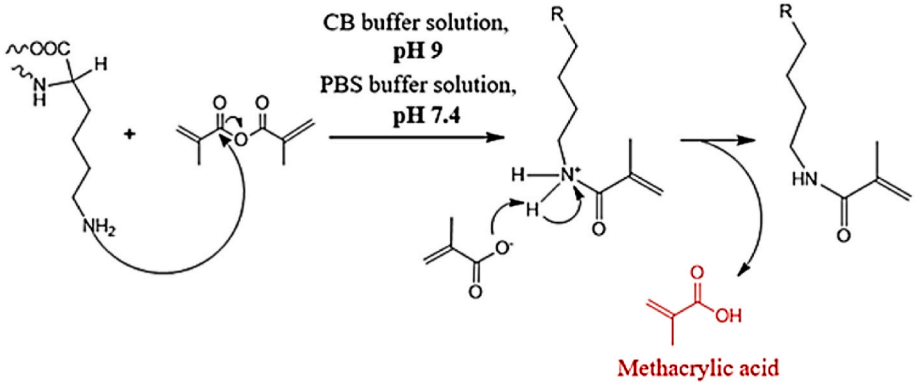

Fig. 1. Schematic representation of gelatin methacryloyl (GelMA) synthesis process. CB: Carbonate-bicarbonate; PBS: phosphate-buffered saline.

with gentle stirring. After 2 h, the reaction was stopped by adding 0.25 ml 1 M HCl and 0.5 ml of sodium dodecyl sulfate (SDS) 10% w/v. The absorption was measured at 335 nm at room temperature by UV–vis spectroscopy using an Evolution 600 UV–vis spectrometer provide by Thermo Scientific. For the analysis, the solution was placed in a 10 mm path length quartz cuvette [24]. Calculation of amino group content was done using a glycine standard curve using a glycine concentration of 0, 1, 2, 3.5, 5, 7 and 10 μg/ml (Fig. S1). The DOF_{TNBS} was calculated using Equation (3):

$$Degree\ of\ functionalization(DOF_{TNSP}) = NH_2\ content\ gelatin\left[\frac{mmol}{g}\right] - NH_2\ content\ GelMA\left[\frac{mmol}{g}\right] \quad (3)$$

2.5. Preparation of GelMA-based biomaterial inks

To prepare the GelMA biomaterial ink, 10% w/v of GelMA powder was first dissolved in PBS (pH = 7.4) at 40 °C, under gentile stirring. This procedure was carried out using the powders of either GelMA_PBS or GelMA_CB previously synthesized and freeze-dried (Section 2.2) to evaluate the impact of the type of buffer on the hydrogel physical properties. Lastly, the photoinitiator (Irgacure 2959) was added at a concentration of 0.5% w/v of the solution. The mixture was subjected to homogenization by magnetic stirring until the photoinitiator was completely dissolved. For GelMA-XG biomaterial inks, after GelMA dissolution, XG at different concentrations was incorporated into the mixture at 40 °C before adding the photoinitiator. Table 1 reports the percentage composition of the different GelMA-XG biomaterial inks.

2.6. Swelling degree and degradation rate

Discs made of hydrogels were obtained by using silicon molds. GelMA and GelMA-XG 20% biomaterial inks composed of either GelMA_PBS or GelMA_CB were used to investigate the influence of buffer solution and XG on hydrogel swelling and degradation rates. More in detail, GelMA-based biomaterial inks were poured into a cylindrical mold with a diameter of 8 mm and a thickness of 3 mm. Then, the hydrogel discs were cured by a UVA lamp having a power of 25 mW/cm^2 for 15 min. To evaluate the swelling degrees and degradation rates, the samples were immersed in PBS and incubated at 37 °C. The swelling degrees were computed by measuring the weight of each sample after removing the residual liquid at predetermined periods of time, i.e., 15, 30 min, 1, 2, 3, 4, 5, and 6 h [25]. The degree of swelling at each time point was calculated using Equation (4):

$$Degree\ of\ swelling\ (\%) = \frac{W_{timepoint} - W_0}{W_0} \times 100 \quad (4)$$

where $W_{timepoint}$ is the weight of the samples at each time point and W_0 is the weight of the samples before immersion in PBS. Once the swelling equilibrium has reached, the samples were incubated at 37 °C and weighed after 1, 3, 5, 7, 10, 14, 21, and 28 days for degradation studies. Before each weighting, the residual liquid around the discs was removed and subtracted from the swelling equilibrium weight using Equation (5):

$$Degradation\ rate\ (DR\%) = \frac{W_s - W_{timepoint}}{W_s} \times 100 \quad (5)$$

where W_s is the weight at swelling equilibrium.

Table 1
Percentage composition of the investigated biomaterial inks. XG: xanthan gum; GelMA: gelatin methacryloyl; PBS: phosphate-buffered saline; CB: carbonate-bicarbonate; wt.: weight; w.r.t: with respect to.

Ink	XG wt.% w.r.t. GelMA	XG wt. %	GelMA wt. %	PBS or CB buffer wt.%
GelMA	0	0	10	90
GelMA-XG 20%	20	2	8	90
GelMA-XG 30%	30	3	7	90
GelMA-XG 40%	40	4	6	90

2.7. Rheological characterization

The rheological characterization was performed using a Discovery HR2 rotational rheometer provided by TA instrument. A cone-plate geometry with a diameter of 20 mm was chosen. All the tests were performed at 25 °C. A conditioning step was performed prior to all tests consisting of a rotation of the tool at 10 s^{-1} for 30 s followed by a soak period of 30 s. Three types of rheological tests were performed: i) a flow curve; ii) a strain sweep and; iii) a frequency sweep. In the flow curve, the shear rate was progressively increased in a logarithmic manner from 0.01 s^{-1} to 1000 s^{-1} while the instrument was recording the shear stress and the viscosity of the material. Ten points per decade were registered and the test time was 180 s, i.e., 30 s per decade. In the strain sweep tests, an oscillatory strain was applied in a logarithmic manner going from 0.1% to 1000%. Ten points per decade were registered. The frequency of the oscillation was kept fixed at 1 Hz. The storage (G') and loss modulus (G'') of the materials were recorded. In the frequency sweep tests, the materials were subjected to an oscillation strain of 1%, while the oscillation frequency was changed from 0.1 Hz to 100 Hz in a logarithmic manner. The value of the oscillation strain was chosen in a way that the materials were in the linear viscoelastic region of the strain sweep curves, i.e., the region of the curve where the moduli are constant with respect to the applied oscillation strain. Ten points per decade were registered. The storage (G') and loss modulus (G'') of the materials were recorded.

2.8. In vitro indirect cytotoxicity

L929 was routinely cultured in complete culture medium composed of DMEM supplemented with 10% FBS and 1% penicillin/streptomycin

antibiotics. Cylindrical hydrogel samples obtained as described in 2.7 were placed in 6-well plates and soaked in 70% ethanol for 4 h followed by washing three times with sterile PBS. Once removed PBS, specimens (N = 3 per time point) were incubated at 37 °C and 5% CO_2 in complete culture medium. The incubated medium was collected after 1, 5, and 7 days of incubation. L929 cells were seeded in 12-well plates at a density of $1x10^5$ cell/well and allowed to reach 70% confluency. Then, to evaluate hydrogel cytotoxicity, complete culture medium was withdrawn and replaced with the same volume of medium previously incubated with hydrogel samples. For control, fresh complete culture medium was added in 3 wells (N = 3). Cells were further cultured for 24 h. After 24 h, alamarBlue™ assay was performed according to the manufacturer's instructions. Absorbance at 570 nm and 600 nm was measured by using a microplate reader (infinite 200Pro, Tecan) and percentage viability was computed.

2.9. 3D printing and printability assessment

For 3D printing, an Inkredible+ printer provided by Cellink was used. The 3D printer is equipped with a dual pneumatic printing head featuring a heated syringe holder. All the prints were performed at 25 °C. Two types of nozzles were used, i.e., cylindrical and conical, with an inner diameter of 25G (0.25 mm). The printability assessment was carried out using a so-called line printing test. A series of lines were printed gradually increasing the speed from 3 to 30 mm/s. The printing pressures used were 20, 25, and 30 kPa for the conical nozzle and 60 and 80 kPa for the cylindrical one. Prior to the printing of the series of lines, two horizontal lines were printed to ensure an adequate extrusion and flow of the material. The width of the line was measured using ImageJ software after imaging the lines with an optical microscope (Eclipse Ti2, Nikon). Based on the results of the line printing test, the printing parameters were selected to print 3D structures thus evaluating the feasibility of fabricating multi-layered scaffolds and assessing the ability to retain their shape. The geometrical details of the structures and the printing parameters are specified in Section 3.5.

2.10. Statistical analysis

Statistical analyses were performed with IBM SPSS software. Two-way ANOVA was employed with a 95% confidence interval. Significant differences were reported for p-values lower than 0.05, with * $p < 0.05$.

3. Results and discussion

3.1. Methacrylation characterization

First, the impact of different solvents, namely PBS buffer solution (pH 7.4) and CB buffer solution (pH 9), on the DOF was evaluated through ^{1}H NMR spectroscopy. For ^{1}H NMR spectroscopy, the two methods indicated and explained in Section 2.3 were employed. Methacrylate functional groups were grafted onto the gelatin backbone through the reaction between methacrylic anhydride, lysine, and hydroxylysine residues resulting in the formation of methacrylamide and methacrylate. In this context, the modification of lysine residues was confirmed by the decrease in the lysine (2H) signal at 2.9 ppm, and by the increase of the methyl group (3H) signal at 1.8 ppm for both GelMA spectra with respect to the gelatin spectrum. Additionally, GelMA spectra revealed the presence of two new signals between 6.1 and 5.4 ppm, corresponding to the acrylic protons (2H) of methacrylic functions as confirmation of methacrylic anhydride functionalization. These two new signals were more evident in the ^{1}H NMR spectrum of GelMA synthesized in the CB solution. Indeed, the intensity of these signals was higher when GelMA was synthesized in the CB solution, indicating a higher DOF (Fig. 2). This result is in agreement with the literature, and it is due to a higher pH of the CB buffer [26]. A higher pH

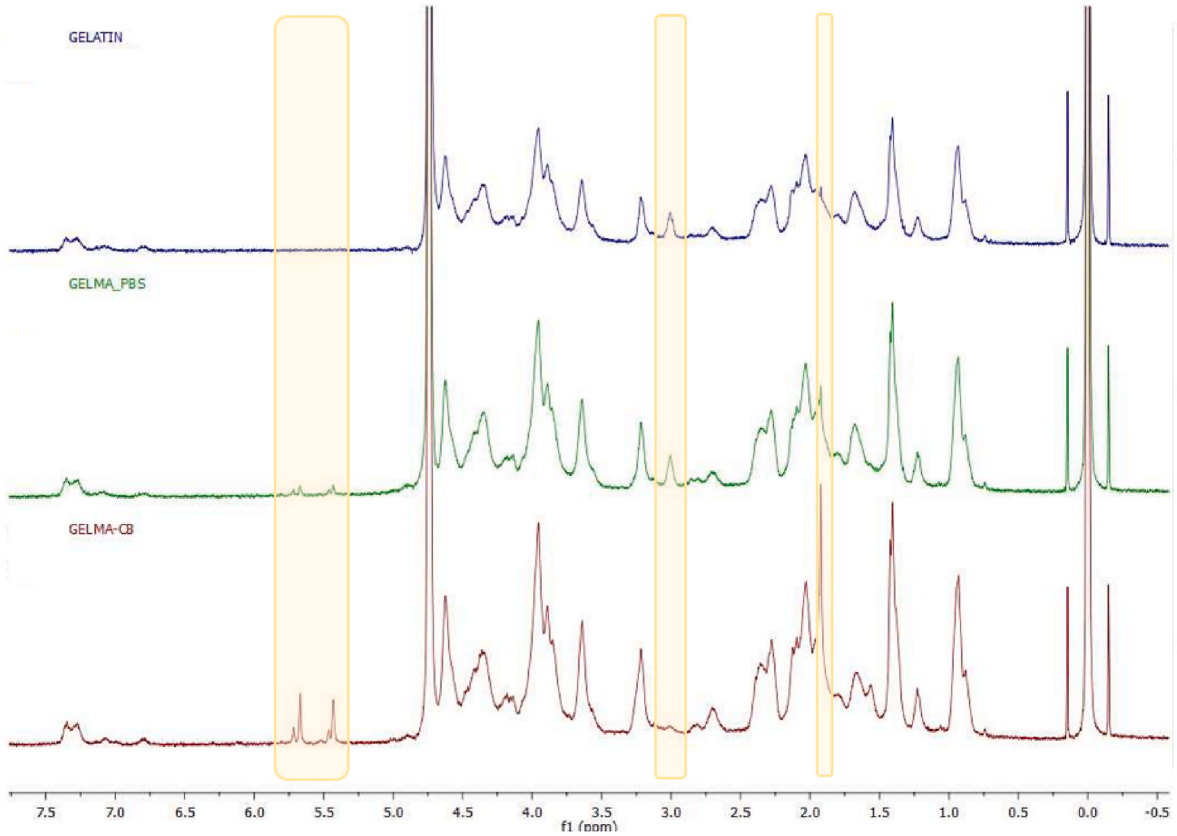

Fig. 2. ^{1}H NMR spectra of gelatin, GelMA synthesized in PBS buffer (GelMA_PBS) and GelMA synthesized in CB buffer (GelMA_CB). In the spectra, the methacrylic functions, lysine, and acrylic function signals are highlighted.

Table 2
DOF computed with the TMSP, lysine, and TNBS method for GelMA synthesized in PBS and CB buffer.

	DOF TMSP	DOF LYS	DOF TNBS
GelMA_PBS (pH 7.4)	33%	29%	36%
GelMA_CB (pH 9)	62%	57%	53%

value enables the reaction solution to stay above the isoelectric point of the gelatin, allowing the methacrylation reaction to occur without being hindered. It would have been possible to increase the DOF values of the hydrogel synthesized in PBS buffer by performing several pH adjustments during the synthesis. However, this strategy would require a high molar excess of methacrylic anhydride. Moreover, it is a laborious method strictly dependent on the operator. The use of the CB buffer, instead, allows obtaining higher DOF without the need for pH adjustments, using a simple one-pot method with high reproducibility [27]. The two different methods used for the determination of the DOF gave comparable results and showed that when using the CB buffer, the DOF almost doubled with respect to the PBS buffer, being the DOF 31% and 59.5% for the PBS and CB buffer, respectively. The latter DOF values were computed by averaging the values obtained via ^{1}H NMR using the TMSP and the lysine methods.

To have an additional quantification of methacrylamide and methacrylate groups in GelMA, a TNBS assay using the Habeeb method was performed. As indicated in Table 2, the DOF values provided by this colorimetric test were consistent with the ones obtained through ^{1}H NMR quantification (Table 2). Indeed, TNBS assay also showed a higher DOF for CB buffer compared to PBS buffer. However, while for the PBS buffer, the DOF obtained with the TNBS assay is comparable with the one calculated through the ^{1}H NMR, in the case of CB buffer the value is lower. The reason behind this result must not be attributed to the material itself nor the measurement approach, but to the lowest sensitivity of the colorimetric assays to GelMA materials with high DOF values [24].

3.2. Swelling degree and degradation rate

GelMA hydrogels may exhibit tailorable swelling and degradation behavior mainly based on the concentration, DOF, and selected curing parameters (light intensity, exposure time of irradiation, and amount of photoinitiator). Here, we assessed if the swelling degree and degradation rate of GelMA hydrogels were affected by different DOF. To this end, GelMA hydrogels were obtained by using either GelMA_PBS or GelMA_CB. The degradation rate is a crucial factor to be considered when developing a new biomaterial ink, as degradation must occur in a timely manner to ensure proper tissue remodeling. Therefore, ideally, the degradation rate should be tuned according to the desired tissue engineering application. All hydrogels exhibited structural integrity after photo-crosslinking. Regarding the swelling rate, all GelMA hydrogels began to swell after 30 min of immersion and reached a swelling equilibrium within 4 h. As shown in Fig. 3, a higher degree of methacryloyl functionalization reached for GelMA synthesized in CB solution led to a lower degree of swelling (16.7% for GelMA_CB, 50.0% for GelMA_PBS). Indeed, a higher DOF implies a higher amount of methacryl groups that are responsible for hydrogel crosslinking upon UV light exposure. Therefore, having a higher amount of methacryl groups increases the crosslinking density, thus decreasing the swelling ratio due to the lower free volume between the hydrogel polymer chains. A lower degree of swelling could be beneficial for the shape fidelity of printed constructs. Concerning the degradation rate, GelMA hydrogels exhibited a trend highly dependent on the achieved DOF. Specifically, the higher the degree of GelMA hydrogels, the slower their degradation rate (Fig. 4). This is related to the fact that a higher crosslinking density due to higher DOF results in a higher amount of covalent bonds and a lower number of physical interactions. As physical bonds are much easier to degrade than chemical bonds, the degradation rate of GelMA_CB hydrogels is lower.

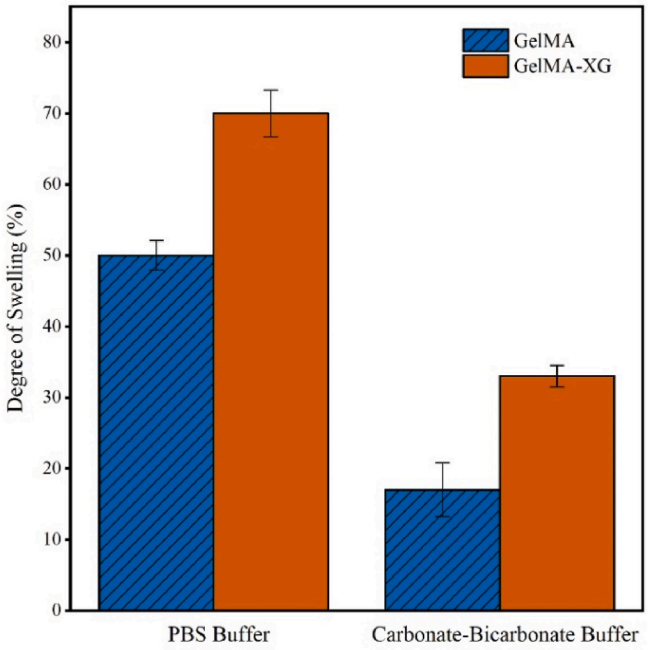

Fig. 3. Swelling degree (%) of GelMA (blue striped bar) and GelMA-XG (orange bar) hydrogels. For all hydrogels, GelMA was synthesized either in PBS or CB buffer solutions. (For interpretation of the references to color in this figure legend, the reader is referred to the Web version of this article.)

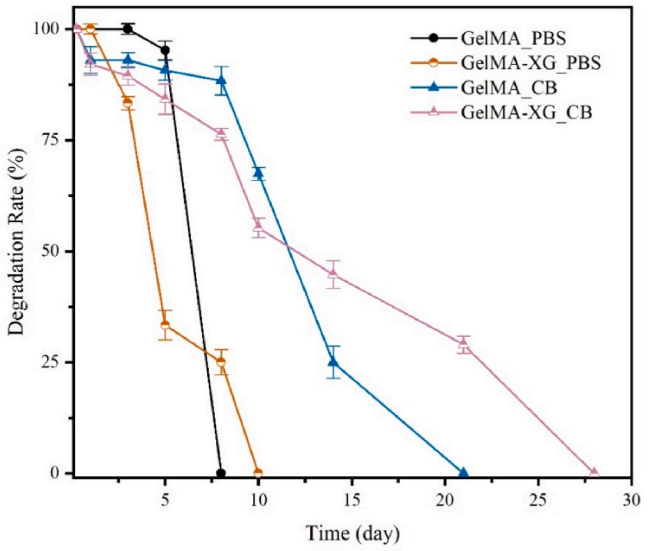

Fig. 4. Degradation rate (%) of GelMA and GelMA-XG 20% hydrogels over time. The analysis was carried out for the following materials: GelMA_PBS (black line), GelMA_CB (blue line), GelMA-XG_PBS (yellow line), and GelMA-XG_CB (pink line). (For interpretation of the references to color in this figure legend, the reader is referred to the Web version of this article.)

The effect of XG on hydrogel physical properties was also evaluated and a 20 wt% concentration of XG with respect to GelMA was first selected for swelling degree and degradation rate tests. XG addition entailed an increase in the degree of hydrogel swelling despite the solvent used for GelMA synthesis and hence, the DOF achieved (Fig. 3). The higher degree of swelling experienced when adding XG may be associated with a higher free volume featured by the hydrogel because of an

overall decreased amount of methacryl groups. Indeed, when considering the biomaterial ink composition shown in Table 1, adding XG decreases the amount of GelMA and hence methacryl groups in the hydrogel, as the total solid content of the hydrogel was maintained at 10% w/v. No meaningful change in the swelling degree was expected by varying the amount of XG, as also reported in the literature [21]. As far as the degradation rate, the presence of XG showed an interesting performance decreasing the hydrogel degradation rate for both GelMA synthesized in PBS and CB (Fig. 4). Therefore, XG seems to improve the overall chemical stability of the hydrogel, delaying the degradation of the material. This phenomenon will be further investigated in future studies.

Based on these outcomes, the swelling and degradation properties of our hydrogels can be easily tuned according to the desired application. For instance, 3D bioprinting has been recently exploited for active drug delivery [28]. Since GelMA synthesized in PBS showed a higher degree of swelling, this material could be employed to produce a drug delivery system able to efficiently incorporate water-soluble drugs thanks to the water uptake capacity. Moreover, drugs could be released with a predictable pattern in vivo over time adjusting the degradation rate. To this end, GelMA chemical stability can be improved by XG addition. On the contrary, GelMA synthesized in CB buffer (with or without XG) was found to be more stable over time, degrading at a slower rate. For tissue engineering applications, the material should degrade fast enough to provide space for cells to deposit new extracellular matrix, but not excessively rapidly such that the mechanical integrity and the initial structure of the printed constructs are not preserved [29]. Also, in this case, XG can be added to control the degradation rate depending on the different target tissues to regenerate. Hence, to better explore the tissue-engineered applications of our new material, we performed the next analyses, including indirect cytotoxicity, rheological, and printing characterization, on GelMA synthesized in CB.

3.3. Rheological evaluation

The rheological properties of the synthesized hydrogels were characterized to qualitatively assess their ability to flow and consequently the extrudability by a pneumatic 3D bioprinter. Fig. 5a shows the flow curves performed on the inks composed of GelMA and different concentrations of XG, as indicated in Table 1. GelMA without XG exhibited a zero-shear rate viscosity of ~10 Pas, then a pseudoplastic behavior was present starting from a shear rate of ~0.1 s^{-1}. At a shear rate of ~100 s^{-1}, the material reached its infinite-shear rate viscosity with a value of 0.03 Pa. With the addition of 20% of XG, the zero-shear rate viscosity increased reaching 500 Pas. The pseudoplastic behavior was still present and the ink reached a minimum viscosity of 0.3 Pa at 1000 s^{-1}. However, in this case, the infinite-shear rate plateau was not present. Furthermore, by increasing the amount of XG, the zero-shear rate viscosity increased as well, reaching a value of 2000 Pas for an XG concentration of 40 wt%. Hence, GelMA-XG inks were characterized by a relatively high zero-shear rate viscosity, that enabled the material to preserve its shape after the printing process thus limiting the filament spreading. The flow curves were fitted using the Carreau-Yasuda model, which takes into account the non-Newtonian behavior of the material and the presence of a zero- and infinite-shear rate viscosity. The model is represented by Equation (6):

$$\frac{\mu-\mu_\infty}{\mu-\mu_0}=\left[1+(k\dot{\gamma})^a\right]^{\frac{n-1}{a}} \quad (6)$$

where μ is the viscosity, μ_∞ the infinite-shear rate viscosity, μ_0 the zero-shear rate viscosity, k the consistency index, $\dot{\gamma}$ the shear rate, n the power law index, and a a parameter describing the transition from the Newtonian region to the power-law region. The values of the model parameters obtained by the interpolations for the studied materials are reported in Table 3.

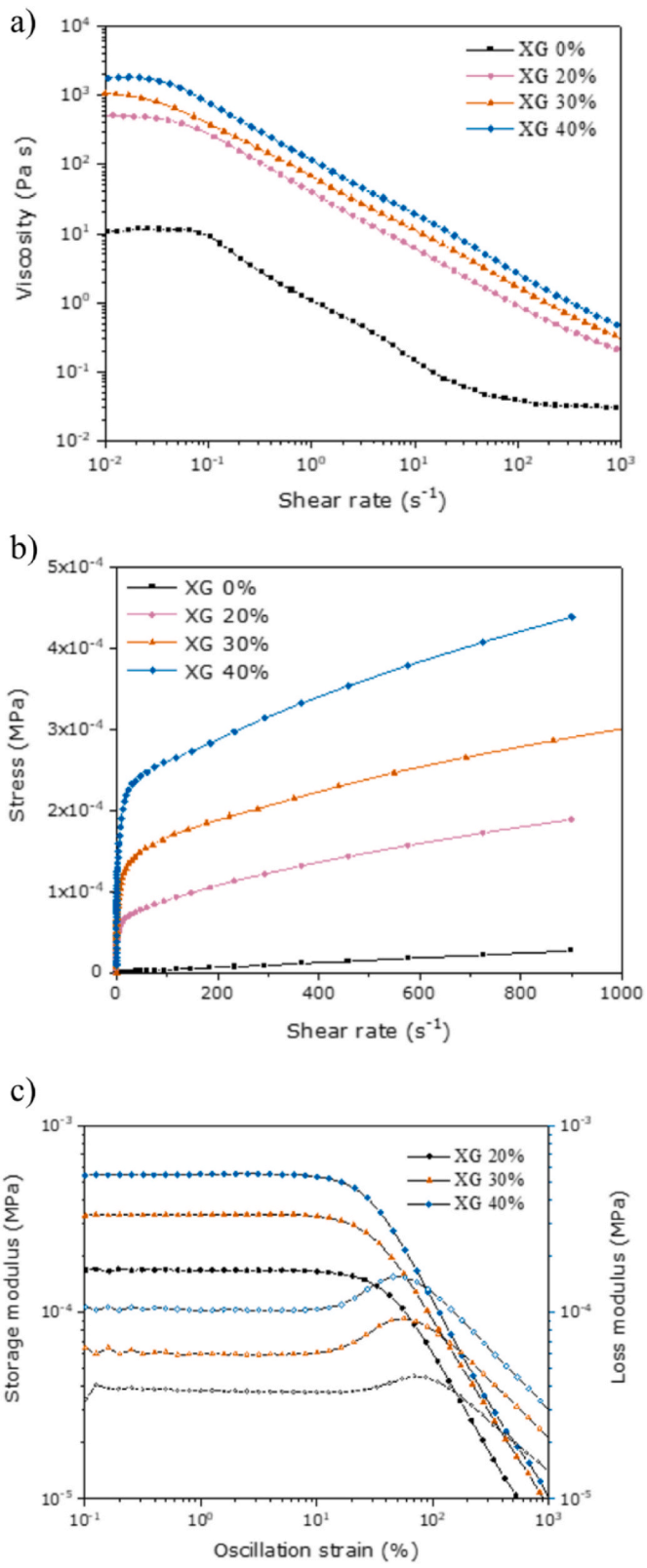

Fig. 5. a) Flow curves showing the viscosity vs. shear rate performed on GelMA with different concentrations of XG. b) Flow curves showing the stress vs. shear rate performed on GelMA with different concentrations of XG. c) Strain sweep tests performed on GelMA with different concentrations of XG.

Fig. 5b displays the stress vs. shear rate curve for the above-mentioned biomaterial inks. All the hydrogels with XG exhibited a clear yield stress, i.e., the stress at which a material starts to flow [30]. In particular, the yield stress values increased along with the amount of XG. On the contrary, the biomaterial ink without XG, instead, did not show any yield stress. Hence, the addition of XG is necessary to obtain a material with a rheological behavior ideal for the extrusion-based printing process. Indeed, the addition of XG endows the biomaterial ink with a shear-thinning behavior, which allows it to be extruded from a nozzle. To further confirm the presence of the yield stress, oscillatory measurements were performed.

The results are shown in Fig. 5c reporting G' and G'' vs. the oscillation strain. When G' is higher than G'', the material displays a solid-like behavior. On the other hand, when G'' is higher than G', the material presents a liquid-like behavior. Therefore, the point in which G' and G'' are equal, also called crossover, represents the yield stress. All the biomaterial inks containing XG exhibited a crossover, thus confirming the presence of a yield stress and their printability. As previously found, it is possible to note also from this graph that the yield stress increased with the concentration of XG. A frequency sweep was also carried out to evaluate the rheological behavior of the materials when the oscillation frequency is changed (Fig. S2). No crossover was present and therefore the material behaved in a solid-like manner over the tested range of frequencies. In agreement with the strain sweep tests, it is possible to observe that both the storage and the loss modulus increased with an increase in the amount of XG.

Based on the rheological characterization and preliminary printing tests, the most suitable biomaterial ink for extrusion-based 3D printing was the one containing 30% of XG. This ink formulation exhibited the best compromise between extrudability and shape retention after printing, as shown in Fig. S3. Therefore, GelMA-XG 30% biomaterial ink was used for the in-vitro biocompatibility assay and printability tests.

3.4. In vitro indirect cytotoxicity

Based on the previous outcomes, the indirect cytotoxicity test was carried out on GelMA and GelMA-XG 30% hydrogels synthesized in CB buffer solutions. The degradation products of both hydrogels did not show any cytotoxic effect. This result agrees with the findings of Zhu et al., who reported that GelMA synthesized in CB buffer solution exhibited cell viability of above 87% [31]. Similarly, cell viability values of GelMA and GelMA-XG 30% hydrogels were higher than 90% for any material incubated for up to 7 days (Fig. 6). No statistical difference was encountered between the viability of controls and cells in contact with GelMA-XG eluates at any time point, whereas on day 1 the viability of cells in contact with GelMA eluates was significantly lower than the viability of controls and cells cultured in GelMA-XG eluates (**p-value <0.01). After 5 and 7 days of hydrogel incubation, a significant difference was found only by comparing the viability of cells in culture with GelMA eluates to the one of controls (*p-value <0.05). It is therefore possible to conclude that degradation products of GelMA hydrogels are non-cytotoxic, thus confirming the effectiveness of the GelMA synthesis process in removing unreacted monomers, which are well known to be cytotoxic above a concentration threshold [32]. Moreover, since to the best of our knowledge the effect of GelMA-XG on cell viability has never been reported before, we preliminarily investigated this aspect here. According to our findings, the degradation products of GelMA-XG hydrogels are non-cytotoxic. This opens the way to its use for cell-based applications. However, further investigations are needed to assess the impact of our biomaterial ink on cell activities and behaviors. To this end, future studies should focus on performing proper cell-based assays to evaluate the viability of encapsulated cells, cell proliferation rate, and the expression of specific markers, thus proving the biocompatibility of the new biomaterial ink.

Table 3
Values of the Carreau-Yasuda model parameters for the investigated materials.

Material	μ_0 (Pas)	μ_∞ (Pas)	k (s)	n	a	R^2
GelMA	10.71	0.026	11.82	0.057	17.27	0.998
GelMA-XG 20%	515.5	0.008	20.5	0.16	2.61	0.999
GelMA-XG 30%	1134.49	0.027	34	0.2	1.67	0.999
GelMA-XG 40%	1718.45	0.004	26.23	0.18	6.56	0.999

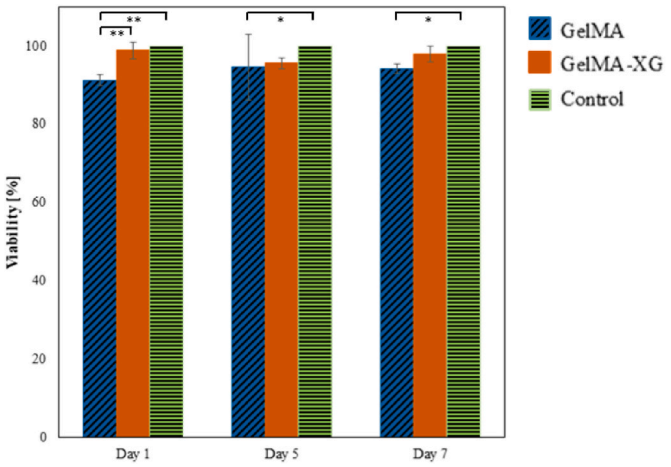

Fig. 6. Viability (%) of L929 cells determined by alamarBlue® assay. The influence of degradation products of GelMA (blue striped bar) and GelMA-XG (orange bar) hydrogels on cell viability was evaluated and compared with control (green striped bar) after 1, 5, and 7 days. Statistical differences are reported with *p < 0.05, **p < 0.01. (For interpretation of the references to color in this figure legend, the reader is referred to the Web version of this article.)

3.5. 3D printing and printability assessment

The printability of the biomaterial inks was assessed by printing an array of lines changing the speed and the pressure. GelMA-XG 30% was selected for the printability test based on its promising rheological behavior and preliminary printability tests. Fig. 7a shows a representative picture of the printability test in which the speed was increased from 3 to 30 mm/s to evaluate the impact of the speed on the filament uniformity and diameter. To this end, the representative microscopy image of a single printed filament is displayed highlighting the filament uniformity. The measurements were repeated by printing the lines with different nozzles and at different pressures to assess the impact of nozzle geometry and pressure values on the printed structure, thus tuning the printing parameters according to the desired application. Fig. 7b represents the trend of the average measured line width obtained with a conical nozzle when increasing the speed. The pressure investigated when using the conical nozzle were 20, 25, and 30 kPa. The line width decreased when increasing the printing speed for all the applied pressures reaching a value of 0.6 and 0.8 mm for a printing pressure of 20 and 30 kPa, respectively. This is due to the lower flow rate that implies a lower material deposition and consequently the printing of a thinner line. Moreover, at a printing speed of 3 mm/s, the average line width ranged between 1.3 and 2.0 mm according to the pressure. As expected, a higher pressure resulted in a higher line width as higher pressures induced higher flow rates. For the same reason, an increase in pressure produced broader lines. It is also possible to observe that the decrease in line width is less pronounced at higher printing speeds, i.e., higher than 15 mm/s. It can be observed that, in all the tested conditions, over-extrusion, i.e., a line width higher than the nozzle diameter, was present. The printability test was carried out also using a cylindrical nozzle with the same diameter as the conical. In this case, the printing pressures were set between 60 and 80 kPa to obtain a proper filament. The decreasing trend of the line width as increasing the printing speed was

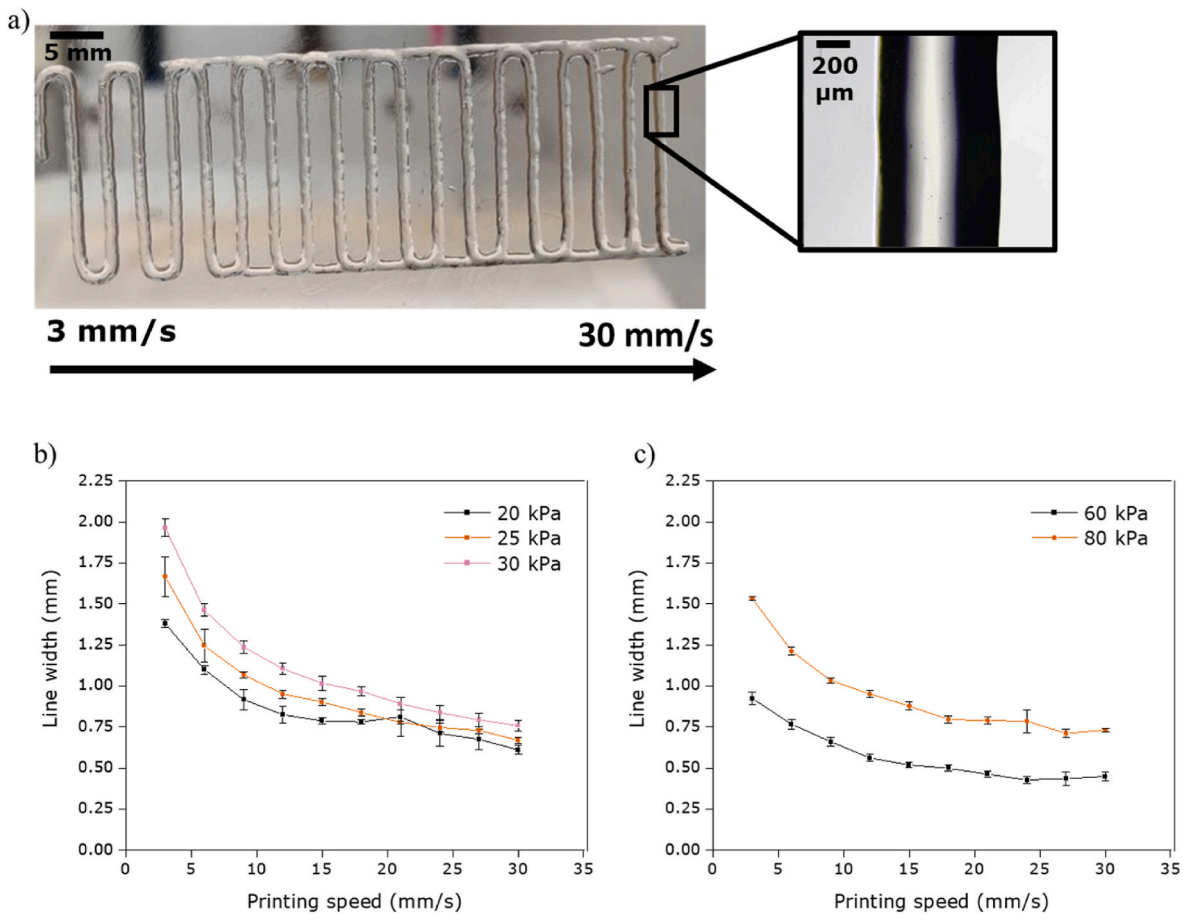

Fig. 7. a) Representative picture of a line-printing test performed with the GelMA-XG 30% highlighting the used printing speeds. A representative microscope image of well-defined lines is also provided. b) Measured line width for GelMA-XG 30% printed at different pressure using a conical nozzle with a diameter of 0.25 mm. c) Measured line width for GelMA-XG 30% printed at different pressure using a cylindrical nozzle with a diameter of 0.25 mm.

encountered also for a cylindrical nozzle, reaching a plateau value after a printing speed of 20 mm/s. Similarly, the average line width resulted to be higher as the pressure increased. Indeed, at a printing speed of 3 mm/s, the line width was 0.9 and 1.55 mm for a pressure of 60 and 80 kPa, respectively, whereas at 20 mm/s it was about 0.4 and 0.75 for a printing pressure of 60 and 80 kPa, respectively. Even in this case, over-extrusion was present in all the tested conditions. It is also important to highlight that over-extrusion can be controlled by changing the printing speed. At low printing speeds, the line width was six times larger than the nozzle diameter, while increasing the speed it was possible to significantly reduce the line width to twice larger than the nozzle diameter. As indicated by higher pressure values involved when using a cylindrical nozzle and the line width measurements, nozzle geometry, i.e., conical and cylindrical, has also an impact on printing conditions and resolution of printed structures. The conical nozzle showed the feasibility of printing the same ink with lower pressure, which is an advantage if inks containing cells need to be printed. Indeed, to obtain a line width of ~1.5 mm printing at 3 mm/s, a pressure of 80 kPa was needed for the cylindrical nozzle, which is almost four times the pressure needed with the conical nozzle. However, the cylindrical nozzle enabled a higher resolution of constructs. Indeed, by controlling the pressure and the printing speed, a lower average line width could be reached when using a cylindrical nozzle compared to a conical one. For these reasons, the selection of the nozzle geometry highly depends on the desired application. For instance, to replicate a capillary network, a better resolution is needed and thus a cylindrical nozzle should be preferred. However, when including cells in the material, the effect of nozzle geometry on cell viability must be considered. According to the literature [33,34], cells are subjected to dramatic stretching and deformation, thus causing cell damage, when a bioink is printed with a cylindrical nozzle due to the sudden change in geometry. Therefore, a conical nozzle should be preferred for printing cells, since it allows the printing of materials with higher viscosities, and it creates printing conditions that are less harmful to the cells.

After the printability test, 3D scaffolds were printed to assess the feasibility of fabricating 3D structures with the GelMA-XG 30% biomaterial ink. Based on the final scaffold aim, which consists in including cells in the material for tissue engineering applications and according to the line printing test a conical nozzle was used. A printing speed of 10 mm/s and a pressure of 25 kPa were selected as the best compromise between filament resolution and uniformity. Scaffolds with a different number of layers and different dimensions were printed. Fig. 8a shows a 1 cm × 1 cm scaffold with five layers right after printing before the crosslinking process. In the structure, no spreading nor filament collapse were observed after the printing process. This confirmed the high shape retention ability of the material even before the crosslinking happened and hence proving that the material is suitable for extrusion-based bioprinting. Fig. 8b displays a 1 cm × 1 cm and a 0.5 cm × 0.5 cm scaffold printed with 10 layers and subjected to UV-curing after the printing process. The result suggests that doubling the thickness of the scaffold did not affect the structural stability and, also in this case, no spreading was encountered while printing. Similarly, the crosslinking process did not alter the scaffold shape. After UV curing, the scaffold was able to preserve macroscopically their shape even when submerged in PBS for 14 days. Moreover, the shape fidelity of the construct was further investigated by significantly decreasing scaffold dimensions. A

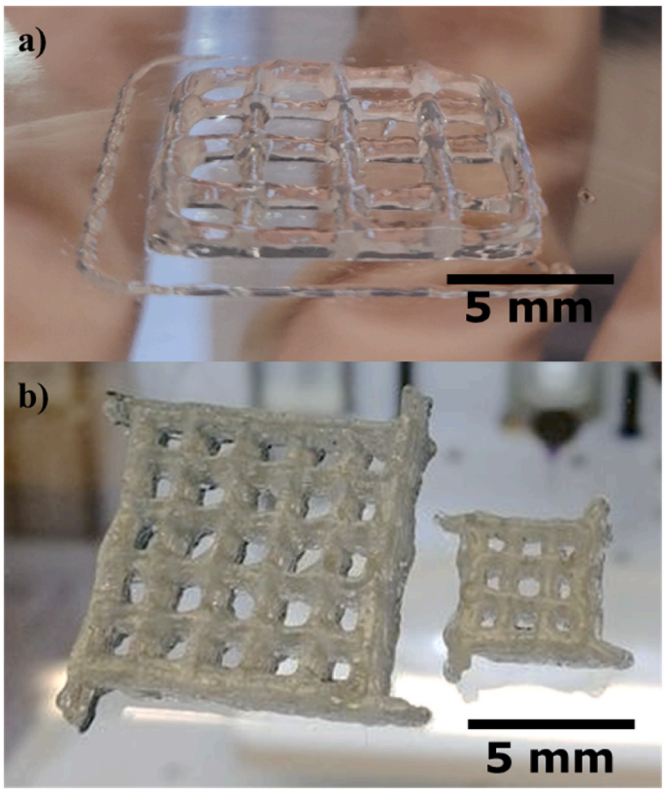

Fig. 8. a) Five-layers scaffold printed with GelMA-XG 30%. b) Ten-layers scaffold printed with GelMA-XG 30% with larger (left) and smaller (right) distances between lines.

0.5 cm x 0.5 cm structure with 10 layers was printed with a minimum line spacing of 0.5 mm. With a lower spacing distance, the lines began to coalesce, making impossible the realization of a proper porous scaffold.

4. Conclusions

The current study focused on the development and characterization of a novel GelMA-XG biomaterial ink for extrusion-based 3D bioprinting. To this end, the impact of different buffer solutions, namely CB and PBS, on GelMA properties was first assessed. According to the results, the CB buffer solution significantly increased the degree of GelMA methacrylation. Due to the higher DOF, the hydrogels based on GelMA synthesized in CB buffer solution showed a lower degree of swelling and slower degradation rate. Hence, the solvent can be selected according to the desired application. For tissue engineering purposes, GelMA synthesized in CB buffer solution ensured higher chemical stability required for a scaffold. Then, the addition of XG to GelMA biomaterial ink was also evaluated in terms of physical properties, printability, and indirect cytotoxicity. Interestingly, the addition of XG seemed to further decrease the degradation rate despite the solvent used. Therefore, the introduction of XG could enable further tuning of the degradability of 3D bioprinted scaffolds according to the application requirements. The optimal combination of GelMA and XG was then assessed through the study of the rheological behaviors of the biomaterial ink and preliminary printability tests. When compared with GelMA biomaterial inks, XG addition increased printability and improved the shape fidelity of the printed constructs. Moreover, here, for the first time, the degradation products of GelMA-XG were proven to be non-cytotoxic. Together, these findings highlight that our newly developed material provides a functional versatile biomaterial ink with suitable printing properties and easily tunable physical properties without causing cytotoxic effects.

CRediT authorship contribution statement

Filippo Iervolino: Conceptualization, Methodology, Formal analysis, Investigation, Writing – original draft, Visualization. **Beatrice Belgio:** Conceptualization, Methodology, Formal analysis, Investigation, Writing – original draft, Visualization. **Aurora Bonessa:** Investigation, Writing – original draft, Visualization. **Federica Potere:** Writing – review & editing. **Raffaella Suriano:** Writing – original draft, Writing – review & editing, Supervision. **Federica Boschetti:** Resources, Writing – review & editing. **Sara Mantero:** Conceptualization, Resources, Writing – review & editing, Supervision. **Marinella Levi:** Conceptualization, Resources, Writing – review & editing, Supervision, Project administration.

Declaration of competing interest

The authors declare that they have no known competing financial interests or personal relationships that could have appeared to influence the work reported in this paper.

Data availability

Data will be made available on request.

Acknowledgments

This research did not receive any specific grant from funding agencies in the public, commercial, or not-for-profit sectors.

Appendix A. Supplementary data

Supplementary data to this article can be found online at https://doi.org/10.1016/j.bprint.2023.e00269.

References

[1] M. Ravi, V. Paramesh, S.R. Kaviya, E. Anuradha, F.D.P. Solomon, 3D cell culture systems: advantages and applications, J. Cell. Physiol. 230 (2015) 16–26, https://doi.org/10.1002/jcp.24683.
[2] M. Rinnerthaler, M.K. Streubel, J. Bischof, K. Richter, Skin aging, gene expression and calcium, Exp. Gerontol. 68 (2015) 59–65, https://doi.org/10.1016/j.exger.2014.09.015.
[3] E. Saygili, A.A. Dogan-Gurbuz, O. Yesil-Celiktas, M.S. Draz, 3D bioprinting: a powerful tool to leverage tissue engineering and microbial systems, Bioprinting 18 (2020), e00071, https://doi.org/10.1016/j.bprint.2019.e00071.
[4] A.K. Badekila, S. Kini, A.K. Jaiswal, Fabrication techniques of biomimetic scaffolds in three-dimensional cell culture: a review, J. Cell. Physiol. 236 (2021) 741–762, https://doi.org/10.1002/jcp.29935.
[5] A.M. Bejoy, K.N. Makkithaya, B.B. Hunakunti, A. Hegde, K. Krishnamurthy, A. Sarkar, C.F. Lobo, D.V.S. Keshav, D. G, D.D. S, S. Mascarenhas, S. Chakrabarti, S. R.R.D. Kalepu, B. Paul, N. Mazumder, An insight on advances and applications of 3d bioprinting: a review, Bioprinting 24 (2021), e00176, https://doi.org/10.1016/j.bprint.2021.e00176.
[6] C. Fan, D.-A. Wang, Macroporous hydrogel scaffolds for three-dimensional cell culture and tissue engineering, Tissue Eng. B Rev. 23 (2017) 451–461, https://doi.org/10.1089/ten.teb.2016.0465.
[7] S.W. Leong, S.C. Tan, M.N. Norhayati, M. Monif, S.-Y. Lee, Effectiveness of bioinks and the clinical value of 3D bioprinted glioblastoma models: a systematic review, Cancers 14 (2022) 2149, https://doi.org/10.3390/cancers14092149.
[8] Q. Gao, B.-S. Kim, G. Gao, Advanced strategies for 3D bioprinting of tissue and organ analogs using alginate hydrogel bioinks, Mar. Drugs 19 (2021) 708, https://doi.org/10.3390/md19120708.
[9] G. Ying, N. Jiang, C. Yu, Y.S. Zhang, Three-dimensional bioprinting of gelatin methacryloyl (GelMA), Bio-Des, Manuf 1 (2018) 215–224, https://doi.org/10.1007/s42242-018-0028-8.
[10] E. Shams, M.S. Barzad, S. Mohamadnia, O. Tavakoli, A. Mehrdadfar, A review on alginate-based bioinks, combination with other natural biomaterials and characteristics, J. Biomater. Appl. 37 (2022) 1–18, https://doi.org/10.1177/08853282221085690.
[11] C.-S. Wang, G. Natale, N. Virgilio, M.-C. Heuzey, Synergistic gelation of gelatin B with xanthan gum, Food Hydrocolloids 60 (2016) 374–383, https://doi.org/10.1016/j.foodhyd.2016.03.043.
[12] M. Sun, X. Sun, Z. Wang, S. Guo, G. Yu, H. Yang, Synthesis and properties of gelatin methacryloyl (GelMA) hydrogels and their recent applications in load-bearing tissue, Polymers 10 (2018) 1290, https://doi.org/10.3390/polym10111290.

[13] A.I. Van Den Bulcke, B. Bogdanov, N. De Rooze, E.H. Schacht, M. Cornelissen, H. Berghmans, Structural and rheological properties of methacrylamide modified gelatin hydrogels, Biomacromolecules 1 (2000) 31–38, https://doi.org/10.1021/bm990017d.
[14] J.A. Benton, C.A. DeForest, V. Vivekanandan, K.S. Anseth, Photocrosslinking of gelatin macromers to synthesize porous hydrogels that promote valvular interstitial cell function, Tissue Eng. 15 (2009) 3221–3230, https://doi.org/10.1089/ten.tea.2008.0545.
[15] J.W. Nichol, S.T. Koshy, H. Bae, C.M. Hwang, S. Yamanlar, A. Khademhosseini, Cell-laden microengineered gelatin methacrylate hydrogels, Biomaterials 31 (2010) 5536–5544, https://doi.org/10.1016/j.biomaterials.2010.03.064.
[16] T. Jain, H.B. Baker, A. Gipsov, J.P. Fisher, A. Joy, D.S. Kaplan, I. Isayeva, Impact of cell density on the bioprinting of gelatin methacrylate (GelMA) bioinks, Bioprinting 22 (2021), e00131, https://doi.org/10.1016/j.bprint.2021.e00131.
[17] H. Li, K. Yu, P. Zhang, Y. Ye, Q. Shu, A printability study of multichannel nerve guidance conduits using projection-based three-dimensional printing, J. Biomater. Appl. 37 (2022) 538–550, https://doi.org/10.1177/08853282221101148.
[18] M. Janmaleki, J. Liu, M. Kamkar, M. Azarmanesh, U. Sundararaj, A.S. Nezhad, Role of temperature on bio-printability of gelatin methacryloyl bioink in two-step cross-linking strategy for tissue engineering applications, Biomed, Materials 16 (2021), 015021, https://doi.org/10.1088/1748-605X/abbcc9.
[19] N. Celikkin, S. Mastrogiacomo, W. Dou, A. Heerschap, E. Oosterwijk, X. F. Walboomers, W. Święszkowski, In vitro and in vivo assessment of a 3D printable gelatin methacrylate hydrogel for bone regeneration applications, J. Biomed. Mater. Res., Part B 110 (2022) 2133–2145, https://doi.org/10.1002/jbm.b.35067.
[20] C. Benwood, J. Chrenek, R.L. Kirsch, N.Z. Masri, H. Richards, K. Teetzen, S. M. Willerth, Natural biomaterials and their use as bioinks for printing tissues, Bioengineering 8 (2021) 27, https://doi.org/10.3390/bioengineering8020027.
[21] Z. Yang, X. Ren, Y. Liu, Multifunctional 3D printed porous GelMA/xanthan gum based dressing with biofilm control and wound healing activity, Mater. Sci. Eng. C 131 (2021), 112493, https://doi.org/10.1016/j.msec.2021.112493.
[22] M.R. Garcia-Cruz, A. Postma, J.E. Frith, L. Meagher, Printability and bio-functionality of a shear thinning methacrylated xanthan–gelatin composite bioink, Biofabrication 13 (2021), 035023, https://doi.org/10.1088/1758-5090/abec2d.
[23] J. Lee, C.H. Park, C.S. Kim, Microcylinder-laden gelatin-based bioink engineered for 3D bioprinting, Mater. Lett. 233 (2018) 24–27, https://doi.org/10.1016/j.matlet.2018.08.138.
[24] C. Claaßen, M.H. Claaßen, V. Truffault, L. Sewald, G.E.M. Tovar, K. Borchers, A. Southan, Quantification of substitution of gelatin methacryloyl: best practice and current pitfalls, Biomacromolecules 19 (2018) 42–52, https://doi.org/10.1021/acs.biomac.7b01221.
[25] B.H. Lee, N. Lum, L.Y. Seow, P.Q. Lim, L.P. Tan, Synthesis and characterization of types A and B gelatin methacryloyl for bioink applications, Materials 9 (2016) 797, https://doi.org/10.3390/ma9100797.
[26] R. Leu Alexa, H. Iovu, J. Ghitman, A. Serafim, C. Stavarache, M.-M. Marin, R. Ianchis, 3D-Printed gelatin methacryloyl-based scaffolds with potential application in tissue engineering, Polymers 13 (2021) 727, https://doi.org/10.3390/polym13050727.
[27] H. Shirahama, B.H. Lee, L.P. Tan, N.-J. Cho, Precise tuning of facile one-pot gelatin methacryloyl (GelMA) synthesis, Sci. Rep. 6 (2016), 31036, https://doi.org/10.1038/srep31036.
[28] J. Lee, A.R. Unnithan, C.H. Park, C.S. Kim, Chapter 5 - 3D bioprinting for active drug delivery, in: A.R. Unnithan, A.R.K. Sasikala, C.H. Park, C.S. Kim (Eds.), Biomimetic Nanoengineered Materials for Advanced Drug Delivery, Elsevier, 2019, pp. 61–72.
[29] X. Barceló, K.F. Eichholz, O. Garcia, D.J. Kelly, Tuning the degradation rate of alginate-based bioinks for bioprinting functional cartilage tissue, Biomedicines 10 (2022) 1621, https://doi.org/10.3390/biomedicines10071621.
[30] H.A. Barnes, The yield stress—a review or 'παντα ρει'—everything flows? J. Non-Newtonian Fluid Mech. 81 (1999) 133–178, https://doi.org/10.1016/S0377-0257(98)00094-9.
[31] M. Zhu, Y. Wang, G. Ferracci, J. Zheng, N.-J. Cho, B.H. Lee, Gelatin methacryloyl and its hydrogels with an exceptional degree of controllability and batch-to-batch consistency, Sci. Rep. 9 (2019) 6863, https://doi.org/10.1038/s41598-019-42186-x.
[32] A.K. Nguyen, P.L. Goering, V. Reipa, R.J. Narayan, Toxicity and photosensitizing assessment of gelatin methacryloyl-based hydrogels photoinitiated with lithium phenyl-2,4,6-trimethylbenzoylphosphinate in human primary renal proximal tubule epithelial cells, Biointerphases 14 (2019), 021007, https://doi.org/10.1116/1.5095886.
[33] S.S. Lee, Y. Yim, K.H. Ahn, S.J. Lee, Extensional flow-based assessment of red blood cell deformability using hyperbolic converging microchannel, Biomed. Microdevices 11 (2009) 1021, https://doi.org/10.1007/s10544-009-9319-3.
[34] T. Tanzeglock, M. Soos, G. Stephanopoulos, M. Morbidelli, Induction of mammalian cell death by simple shear and extensional flows, Biotechnol. Bioeng. 104 (2009) 360–370, https://doi.org/10.1002/bit.22405.

Glossary

1H NMR: proton nuclear magnetic resonance
CB: carbonate-bicarbonate
D_2O: deuterium oxide
DMEM: high glucose Dulbecco's modified eagle's medium
DOF: degree of functionalization
ECM: extracellular matrix
G': storage modulus
G'': loss modulus
GelMA: gelatin-methacryloyl
MA: methacrylic anhydride
PBS: phosphate-buffered saline
RGD: three-amino acid sequence Arginine–Glycine–Aspartate
SDS: sodium dodecyl sulfate
TMSP: trimethylsilyl propanoic acid
TNBS: trinitrobenzene sulfonate
XG: xanthan gum